Applied Surface Science 693 (2025) 162688

Contents lists available at ScienceDirect

Applied Surface Science

journal homepage: www.elsevier.com/locate/apsusc

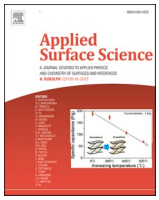

Full Length Article

Surface conductivity of air-exposed hydrogenated diamond: A survey into the subsurface electronic structure and the role of oxygen-related adsorbates

Stefano Iacobucci [a,*], Valerio Serpente [b,c], Daniele Paoloni [b], Daniele M. Trucchi [c], Francesco Offi [b], Alessandro Ruocco [b]

[a] CNR-ISM, Istituto di Struttura della Materia del Consiglio Nazionale delle Ricerche, Via del Fosso del Cavaliere, 100, I-00133 Rome, Italy
[b] Dipartimento di Scienze, Università degli Studi Roma Tre, Via della Vasca Navale 84, I-00146 Rome, Italy
[c] CNR-ISM, Istituto di Struttura della Materia del Consiglio Nazionale delle Ricerche, Via Salaria, Km 29.300, I-00016 Monterotondo Scalo, Rome, Italy

ARTICLE INFO

Keywords:
Hydrogenated diamond
Surface conductivity
Hydrogenation
Atmospheric adsorbates
Structural and electronic properties
Electron spectroscopies

ABSTRACT

The surface conductive and insulating states of microwave plasma hydrogenated diamond (HD) single crystal (1 0 0) surfaces have been investigated by using electron diffraction, electron energy loss and photoemission spectroscopies. Before each experiment, the surface was exposed to air and left to reach the conductive state; then, after measurements, the sample was annealed in ultra-high vacuum, its surface reached the insulating state, and the measurements were repeated. We have determined coherently scattering domains average dimension of (2×1) reconstructed HD surfaces both in insulating and conductive state, resulting in a smaller dimension in the latter case, due to adsorbates inducing surface conductivity. Airborne adsorbates containing oxygen, which actively contribute to enhancing surface conductivity, are randomly distributed and cover about 23 % of the surface. Monte Carlo simulations show that the hydrogenation process produces hydrogen penetration beyond the topmost surface layer; this result supports X-ray core-level photoemission spectroscopy data interpretation. The role of oxygen and oxygen-related adsorbates in the surface conductivity of hydrogenated diamond has also been studied by using controlled exposure to atomic oxygen. We have found that oxygen adsorbs on the surface without bonding to carbon. This behavior contrasts with that of airborne adsorbates, which are the primary contributors to surface conductivity.

1. Introduction

Diamond is characterized by remarkable mechanical, chemical and physical properties [1,2], and the progress in their full exploitation is governed by challenges on both material production and deep comprehension of its characteristics. Among the extreme and unique features of diamond that enable applications in a variety of fields – from biological and chemical sensing [3] to thermionic emitters [4,5] and solar absorbers [6,7] – one of the most fascinating is the enhanced electrical (p-type) surface conductivity exhibited when hydrogen-terminated, which is several orders of magnitude higher than the bulk one [8]. Ever since its discovery in 1989 [9], the surface conductivity (SC) of hydrogenated diamond (HD) has been the subject of intensive studies, aiming both at the comprehension of the basic mechanism and its technological exploitation. The two-dimensional (2D) character of the SC has been proven by a low-temperature characterization of diamond in-plane gated field-effect transistors [10]; although it has been successfully used for high-power and high frequency electronic devices [11,12], with potential applications in spintronic applications [13], and even though stabilizing coatings are under development [14], a complete explanation for the basic mechanisms responsible of the SC in HD has remained elusive.

After the milestone experiment of Maier [8], which shed light on the necessity of both H termination and exposure to air to induce conductivity in the diamond surface, and formulated a first electrochemical model to explain its origin, the topic has been the subject of debate [15]; further models have been developed with differently articulated approaches [16–18], contextualizing the mechanism of the SC in HD as a specific case of a more general phenomenon – the adhesion of water on otherwise hydrophobic surfaces – particularly pointing out the

* Corresponding author.
E-mail address: stefano.iacobucci@ism.cnr.it (S. Iacobucci).

https://doi.org/10.1016/j.apsusc.2025.162688
Received 3 December 2024; Received in revised form 4 February 2025; Accepted 12 February 2025
Available online 15 February 2025

relevance of the chemical state of the surface itself [19]. The establishment of SC requires that an additional adsorbate on the HD surface should act as an acceptor in order to create a 2D charge accumulation region and there is a general consensus that charge carriers are holes at up to few nanometer depth under the surface [20]. Such surface transfer doping gives rise to a fundamentally altered surface electronic structure from that of the bulk, as demonstrated by photoemission experiments supported by *ab-initio* density functional calculations, showing that in air-exposed (100) surfaces carriers are organized in a twofold band structure, with effective masses of about one half and twice the electron rest mass, respectively [21].

SC represents a specific topic of the more general theme of hydrogen interactions with diamond, because H can be entrapped in the diamond bulk during growth. In such a context, many investigations have been performed to clarify C–H bonding configuration and concentration and its influence on the chemical and physical properties of the host diamond matrix [22]. Likewise it is known that H-passivation of the diamond surface produces negative electron affinity (NEA) [23,24] by inducing a surface dipole layer, an energetic condition that favors the charge transfer responsible for the enhanced SC [25]; in this regard, it has been both experimentally and theoretically investigated how not only the hydrogen deposited on the diamond top layer but also the subsurface hydrogen atoms may contribute to enhancing SC [26–29].

Besides this, the quizzing topic of which adsorbed molecular species is responsible for the surface charge transfer remains unanswered. This question has pushed for investigations aiming at stabilizing and maximizing the carrier sheet density by controlled adsorption and desorption of selected chemical molecules on both hydrogen- and deuterium-terminated diamond [30–34], as well as by film deposition of transition metal oxides both in ultra-high vacuum (UHV) [14,35–39] and using solution-processed methods [40]. According to Kubovic's results [30], the most efficient species present in the atmosphere are all strong oxidant ones. This is not a trivial finding, insofar as oxygen itself exists in the atmosphere in molecular state and is present in several bonding configurations with hydrogen and carbon [41,42]; it is also worth noticing that these oxygen-related sites can contribute directly to the transfer-doping mechanism as argued by Maier [8], Bobrov [26], Sque [42], and/or act as catalysts as suggested by Riedel.[43].

It has been recently reviewed how interface details with electron accepting species modify in a striking way sheet resistance and characteristics of the resulting 2D hole gas [44]. In this context, it is mandatory to investigate the influence of the airborne adsorbates on the SC of HD, particularly the characterization of the C–H bond, as well as the specific role of oxygen, achieved by correlating macroscopic properties with electronic structure. This approach has already been fruitfully exploited: fine structures in photoelectron yield from HD surface have been identified as signatures of the loss and recovery of SC upon annealing in vacuum and exposure to different kinds of atmospheres [43]; the surface electronic structure of HD has been correlated with conductivity measurements by STM experiments [26]; spin–orbit interaction in the 2D-hole gas at the diamond surface has been linked with magneto-conductivity experimental results [45]; differences in valence band structures at Fermi level for bulk and surface HD corresponding to the insulating and conducting state of HD, respectively, have been highlighted [21].

In this work, we compare macroscopic and microscopic properties of diamond samples hydrogen-terminated *ex-situ* by microwave H-plasma. The sample conductive state has been correlated with elemental and morphological analysis by surface-sensitive techniques: scanning angle low energy electron diffraction (SA-LEED), electron energy loss spectroscopy (EELS) and X-Ray Photoemission Spectroscopy (XPS) to investigate the C–H and C-O bond, performing experiments on conductive (air-exposed), non-conductive (*in vacuum* annealed) and after controlled O-exposure of HD sample surface.

2. Experimental methods

Hydrogenation and electrical characterization have been performed at the DiaTHEMA laboratory of the CNR-ISM on two single-crystal (100) commercial (Element Six Ltd) diamond squared plates (4.5×4.5 mm^2 surface area, 0.5 mm thickness), characterized by a minimal presence of impurities, called sample A and sample B. Sample A is a standard grade sample (with nitrogen and boron atomic concentrations < 1 and < 0.05 ppm, respectively); sample B is an electronic grade sample (with nitrogen and boron atomic concentration < 5 and < 1 ppb, respectively). Sample surfaces have been cleaned by acid treatment according to standard protocols as in ref [46] and hydrogenated in a microwave chemical vapor deposition (CVD) customized ASTeX S1500 reactor (substrate temperature of 700 °C, gas pressure of 40 mbar, microwave power of 1.2 kW, treatment time of 1 h).

To study the penetration depth of H ions into the diamond lattice during the plasma treatment, we have performed Monte Carlo simulations of the hydrogen plasma process in terms of collisions of H particles accelerated by a (equivalent) potential difference between the sample surface and the plasma reactor and subsequent implantation into the diamond lattice. To do this, we have used the SRIM 2013 software [47], in which every simulation consists of 10^5 ions impinging onto the diamond sample with a fixed angle and a kinetic energy corresponding to the potential difference between the sample and the H source.

Hydrogenated samples have been removed from the CVD chamber and exposed to air. Surface roughness of about 5 nm for the sample A and of about 0.5 nm over 1 μm radius (average value) for the sample B has been measured by AFM, respectively [48]. Electrical measurements have been performed in a high-vacuum and temperature electronic characterization apparatus, where a huge jump in resistance (from a few tens of kΩ up to a few TΩ) was registered upon annealing from room temperature (RT) up to over 500 °C. Resistance remained in the TΩ range after cooling the sample back to RT and dropped down to its initial value in few hours upon sample exposure to air. The reversibility of the switch from high- to low-conductivity regime has been verified by repeating the electrical measurements after exposure to air and subsequent new annealing in vacuum. Details of the experimental setup and procedure can be pinpointed in [49]. These findings, while comparing to Maier's results [8], provided us with a reliable recipe to prepare sample surfaces in conductive (air-exposed) and non-conductive (in vacuum annealed) regimes to be measured in the electron spectroscopy equipment.

The apparatus for electron spectroscopy experiments is located in the LaSEC laboratory of Roma Tre University [50]. Briefly, it consists of two UHV vessels in communication: a preparation and a main chamber. The main chamber hosts a monochromatized X-ray source and twin electron spectrometer (performing an overall XPS energy resolution of about 400 meV in the present work). All photoemission spectra have been acquired by using a pass energy of 40 eV, except for the C 1s spectra reported in Fig. 5 with the corresponding fits, which have been measured with a 20 eV pass energy. The main chamber is also equipped with a custom-made electron gun (e-gun) with an energy resolution of few tens of meV and low-to-mid current emission (10^{-13}–10^{-7} A). Its current emission is not a trivial characteristic in order to exclude radiation and electron-related damage, a well-known issue associated with the metastability of most allotropic forms of C upon electron bombardment [51]. We have used an e-gun current density of about 10^{-11} A/mm^2 to perform EELS spectra, verifying reproducibility to exclude surface degradation due to electron irradiation. We have also used the e-gun in combination with the electron analyzer to perform SA-LEED: the electron diffraction patterns have been obtained by scanning the sample polar angle while the electron spectrometer detected the rate of elastically scattered electrons at a fixed energy. Details of the technique can be found in [52,53]. Finally, the electron source has been also used as a flood-gun to preserve the net charge in the target area during XPS measurements on the non-conductive diamond surface: specifically, we increased the current (up

to an integrated intensity of few tens of nA, with 50 eV of kinetic energy) until we measured that core level binding energy no longer changed. The apparatus is also equipped with a temperature controlled five-axis manipulator, whose head is supplied with a tungsten filament used for sample annealing. The preparation chamber hosts a fast-entry system for sample introduction from air, a mass spectrometer for residual gas analysis and a conventional low-energy electron diffraction (c-LEED) system. Moreover, an oxygen dissociation system allows introducing molecular oxygen into the prep-chamber in a controlled fashion and to dissociate it by thermal cracking produced by a hot tungsten filament placed at a few centimeters from the sample.

In this work, SA-LEED measurements have been performed on sample A, EELS and XPS on sample B. Following the recipe previously described, after hydrogenation both samples have been exposed to air for more than 12 h to achieve the surface conductive state. Then, they were measured and subsequently annealed in UHV at 450 °C to bring the surface to the non-conductive state and a new cycle of measurements has been taken. After that, XPS has been performed on B sample after controlled exposure to molecular O_2 and atomic O. The percentage of O with respect to O_2 has been checked by the mass spectrometer. Possible deposition of spurious oxide species on the sample, a critical issue of the method [54], has been found to be below the XPS detection limit.

3. Results and discussion

SA-LEED experiments have been used to determine the surface long-range order of HD samples in both the conductive and non-conductive states, providing insights into the effects of the atmospheric adsorbates on the system morphology. Fig. 1 displays the diffraction pattern acquired at RT for 100 eV electrons, which are expected to provide surface sensitivity [55]. The two profiles are the measured intensities as a function of the parallel momentum exchanged during the angular scan – (0,0) corresponding to the specular reflection – for both conductive and non-conductive surfaces: the black line has been measured on the sample after air exposure and insertion into the UHV system, the red line has been measured after annealing in UHV. In the inset of Fig. 1 an example of c-LEED image measured on the annealed surface is also reported. The diffraction pattern of the (2 × 1) reconstruction, characteristic of the (100) HD surface [56], is clearly identifiable both in the diffraction profiles and the c-LEED image. In particular, the profiles acquired by SA-LEED along the direction corresponding to the dashed line in the c-LEED image allow for an analysis of the sample surface order by a comparison of the non– conductive and conductive surfaces on a quantitative ground. While the diffraction peak positions are unchanged, a higher signal-to-background ratio is evident in the non-conductive surface with respect to the conductive one.

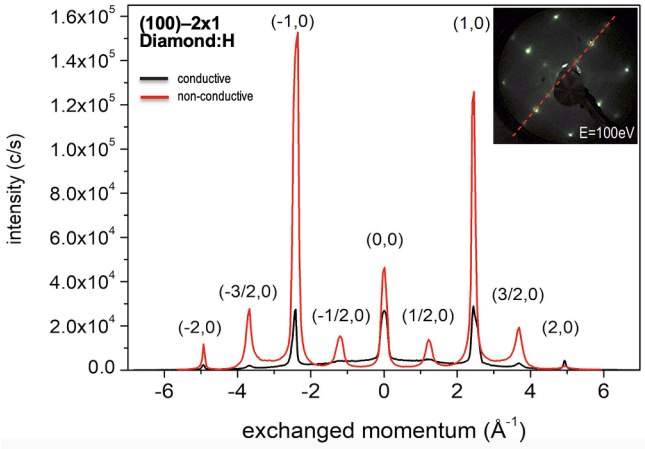

Fig. 1. SA-LEED profiles of (air-exposed) conductive (black line) and (annealed) non-conductive (red line) hydrogenated diamond (100)-2x1 surfaces, respectively. (0,0) corresponds to the specular reflection; half-integer label peaks are associated with the surface reconstruction. In the inset, the correspondent 2D pattern measured on the non-conductive surface by a c-LEED system is also reported: the red dot-line indicates the scan direction of the sample polar angle along which the intensity distributions of the main figure are measured. Both SA-LEED and c-LEED experiments have been performed with 100 eV electrons. (For interpretation of the references to colour in this figure legend, the reader is referred to the web version of this article.)

By a fitting analysis of the diffraction patterns with a procedure described in [52,53], a quantitative estimation of the coherently scattering surface domain dimension has been done. The analysis is reported in Fig. 2, top panel for the non-conductive (annealed) state and bottom panel for the conductive (air exposed) state, respectively. The best fit of the non-conductive diffraction pattern is obtained via the sum of two signals given by surface (2 × 1) reconstruction and bulk diamond (purple shaded and green lines, respectively). Both (2 × 1) reconstruction and bulk diamond signals are composed by a sum of peaks with equal Voigt line shape, whose positions are correlated, being expressed as a multiple of the reciprocal unit vector. In this way, the exchanged parallel momentum of the (−1,0) peak is equal to twice the one of the (−1/2,0) peak. In the Voigt profiles, the Gaussian width that is due to the apparatus transmission function has been imposed to be equal for all the peaks. The Lorentzian contribution is related to the sampled domain properties: the diameter of ordered domains is $D = 4\pi / l$, where l is the full width at half maximum of the Lorentzian function [57]. The fitting

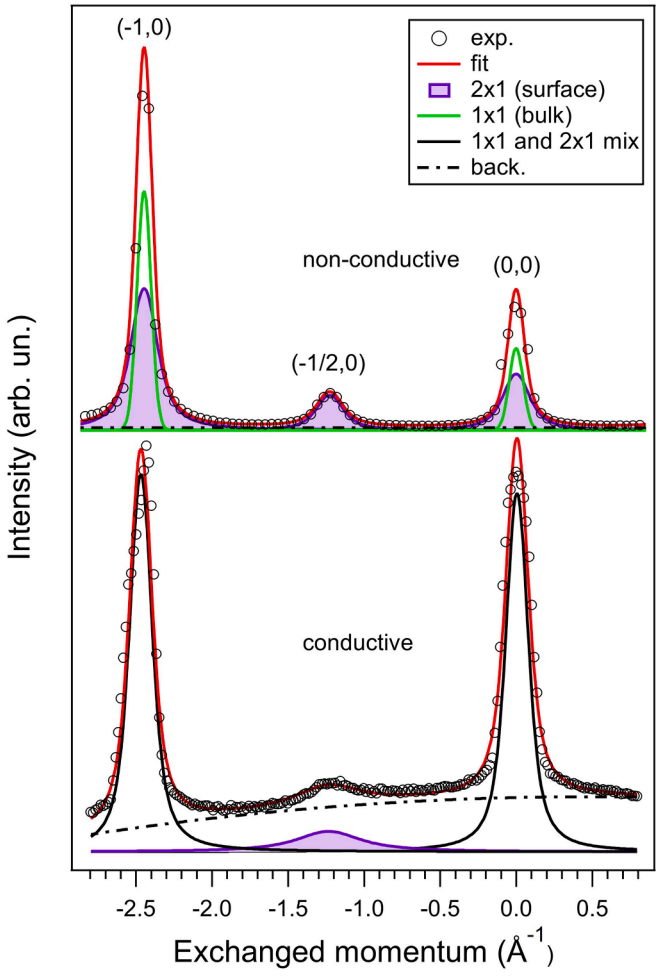

Fig. 2. Best fit of the electron diffraction patterns of the non-conductive (annealed) (top panel) and conductive (air-exposed) (bottom panel) HD surfaces (see text for explanation). Intensities have been normalized to the (−1,0) peak for better visualization.

Lorentzian width of bulk signal is zero, hence the corresponding diameter is found to be infinite. Within the same procedure we obtain from the Lorentzian width of the (2 × 1) reconstruction signal the determination of reconstructed domains dimension to be (95 ± 35) Å for the non-conductive state.

In the bottom panel of Fig. 2 the diffraction pattern measured on the surface in the conductive state with its fit analysis is reported. We observe background increasing and diffraction peak broadening with respect to the same sample in the insulating state. Both findings may be ascribed to a disordered adsorption of the airborne species. In the non-conductive sample pattern there is a very low intensity constant background, while in conductive state is necessary to introduce a two-degree polynomial one, suggesting that the disordered distribution of adsorbates generates an incoherent scattering that results in the broad bump centered at exchanged parallel momentum equal to 0. The presence of adsorbates, with the consequent dampening of surface reconstruction, makes the fitting procedure more complex. We fit the (0,0) and (−1,0) peaks with a single component (black line), because it is not possible to distinguish the signal given by surface (2 × 1) reconstruction from the bulk diamond one. Moreover, from the width of the (−1/2,0) peak it is possible to determine the diameter of reconstruction domains which is (25 ± 5) Å. The decrease in the diameter of the reconstructed domains suggests that adsorbates alter the structure and morphology of the areas where the diamond is hydrogenated, reducing their degree of order.

Such SA-LEED quantitative results add a piece of information to shed light on the role of the airborne adsorbates. Indeed, the size of hydrogenated coherently scattering domains, both in the conductive and non-conductive states, is a novel information that can be used in studies aimed at modeling the surface conductivity induced by adsorbates. Moreover, these measurements open up possible paths for further experiments, investigating the correlation between the size of the domains and the transport mechanisms for example in the thermally induced desorption of adsorbates, where hopping mechanism can occur.

Inelastic electron scattering experiments correlated with the surface conductivity state provide us with information on modifications of the electron excitations induced by the interaction with airborne adsorbates. EELS measurements, performed in specular reflection at RT are shown in Fig. 3. The black square and the red profiles have been measured on the conductive (air-exposed) and non-conductive (annealed) surfaces, respectively. In both spectra, typical losses of hydrogenated crystalline diamond can be recognized. The low loss region (up to 8 eV) is a benchmark of the surface chemical termination: according to previous works [58] the hydrogen- (deuterium-) terminated surface shows an EELS spectrum characterized by a gap in the (2–6) eV-energy range (P1 bandgap): our data can be accordingly interpreted. A small inflection faintly visible at about 10 eV energy loss signals a small oxygen contribution [59]. An inter-band transition between the valence and the conduction bands contributes to the P2 feature at about 14 eV [60] and the P3 and P4 structures at about 22 eV and 33 eV correspond to the surface and bulk plasmons [61], respectively. Notably, P3 and P4 structure intensities are reduced in the conductive state sample spectrum, due to the presence of the airborne adsorbates.

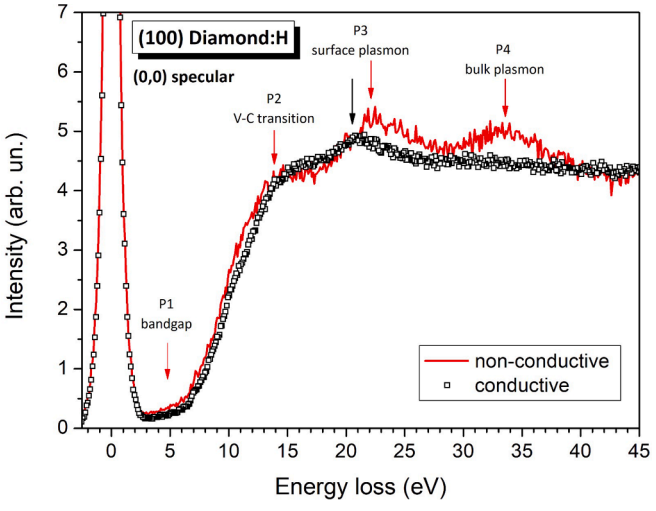

Fig. 3. EELS spectra of HD surface measured in the high-hydrogenation area of the sample [49], which is associated with a high electrical conductivity surface region, in the conductive (black squares profile) and non-conductive (red line) states. Spectral structures are labeled according to Refs. [58–61]. (For interpretation of the references to colour in this figure legend, the reader is referred to the web version of this article.)

Furthermore, there is a 1.5 eV energy shift of the P3 peak in the conductive surface. Occurrence and sign of surface plasmon energy shift are coherent with the presence of an overlayer, as already observed on an organic/inorganic interface system [62] and explained by the model derived by Raether.[63] According to that explanation, in our case it can be argued that the airborne adsorbate dielectric response modifies the frequency of the surface plasma wave propagating in the hydrogenated diamond substrate, thus generating interface plasmons revealed at lower energy losses.

A characterization of the surface chemical state has also been performed via XPS on the non-conductive as well as on conductive HD samples. Fig. 4 (top panel) shows a comparison between the C 1s XPS lines as measured on conductive (black squared line) and non-conductive (red dotted line) samples. At first glance the two spectra look similar, showing comparable line shape and intensity, as well as peak to background ratio; transition from the non-conductive state (annealed sample) to conductive (air-exposed sample) produces an energy shift, which is ascribable to band bending effects;[21,42] the shift has the same sign as and is of comparable amount (about 1.2 eV) to photoemission results on MoO_3 –covered HD surfaces [35].

Oxygen is present in both sample states, as displayed in Fig. 4 (bottom panel) where a comparison between the O 1s core level spectrum measured on conductive (black squared line) and non-conductive (red dotted line) diamond surfaces, respectively, is shown. The O 1s energy shift is comparable with the C 1s one.

We guess that the detected oxygen is mainly localized on the surface; this assumption is supported by angle dependence of the XPS spectra that will be discussed later. Thus, the fraction of the surface covered by oxygen can be estimated by using the Fadley's model [64]. By assuming an inelastic mean free path of 19 Å in diamond for C 1s photoelectrons excited by the Al-Kα line [65], a value of (33 ± 3) % for the fraction of diamond surface covered by oxygen in the non-conductive state is derived. This oxygen persisting after annealing is more strongly bonded to the surface and it does not contribute to SC. We estimate an oxygen coverage of 56 % of the surface in the conductive sample. Thus, we obtain the percentage of oxygen responsible for diamond SC ("active" oxygen) by subtracting the (areal) intensity of the O 1s peak measured on the annealed surface from the one measured on the air-exposed surface. Namely, we determine the O "active" coverage by subtracting from the conductive state surface coverage (56 %) the coverage of non-active oxygen (33 %, measured on the non-conductive sample). In this way we retrieve an "active" coverage of about 23 %, corresponding to the 40 % of the total amount of oxygen on the air-exposed surface, which induces a hole sheet density at RT of 8×10^{12} cm^{-2} on the conductive state, measured by Hall effect. The measured hole sheet density is coherent with the values provided in literature for air-exposed HD, which does not exceed values of about 1×10^{13} cm^{-2} at RT and is far lower than the 2.5×10^{14} cm^{-2} achieved with WO_3 coatings [36] and other high electron affinity oxides [66].

Significant information from core level measurements is also obtained by line-shape analysis. The C 1s line measured on the non-conductive (annealed) surface is displayed in Fig. 5a together with its deconvolution; it is centered at 286 eV of binding energy and it is rather

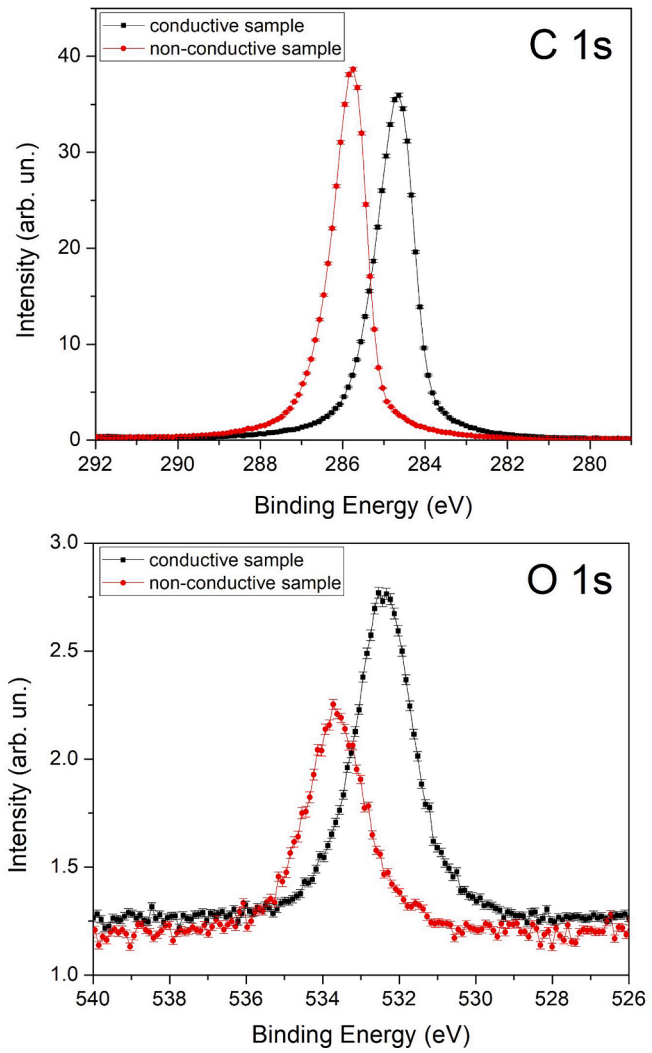

Fig. 4. Comparison between C 1s (top panel) and O 1s (bottom panel) XPS lines measured on the conductive (black squares line) and non-conductive (red dots line) diamond surfaces, respectively. (For interpretation of the references to colour in this figure legend, the reader is referred to the web version of this article.)

symmetric apart from a bump at higher binding energy. In the (100) surface, this asymmetry is attributed to a contribution of H-terminated C sites, [67] or to subsurface C atoms not bonded to H.[68].

In order to obtain a detailed description of the component contributions to the carbon spectrum, we have fitted the peak of the C 1s line with a bulk component (C_B) related to carbon in sp^3 configuration and the bump at higher binding energy with a peak C_x (we refer to the sites associated to C_x component as "x" due to the unclear origin of this signal). Following Graupner's interpretation [67] we have fixed the C_x shift at 0.5 eV relative to C_B.[1]

However, Graupner's deconvolution did not consider the possible presence of strongly bonded oxygen on the HD surface. In our case, instead, the significant presence of oxygen has forced us to introduce oxygen-related components in the C 1s fit. Relying on previous XPS investigations on oxygen-terminated diamond [69,70], we have used Voigt profiles and a Shirley background: the Lorentzian width is fixed at 0.15 eV, as done in references;[67–69] the Gaussian width is a free parameter of the fitting procedure and it is broader than the experimental energy resolution due to the presence of unresolved contributions. Best fit peak positions are the following: C_B and C_x are located at 285.9 eV and 286.4 eV, respectively; C_C is assigned to surface carbon not bonded with hydrogen and to defects (as in ref [67] it is shifted by −0.9 eV with respect to C_B); C_{O1} and C_{O2} are associated to single bonded carbon (i.e. C-O, hydroxyl groups C-OH, ether functional groups C-O-C), shifted by 1.3 eV respect to C_B, and to double bonded carbon (i.e. C=O, O-C-O, carbonyl functional groups >C=O) [71], shifted by 2.5 eV, respectively.

To study the nature of the C 1s components, as just defined in relation to Fig. 5, we have also performed XPS measurements as a function of the collection angle of photo-emitted electrons, with the concept that grazing collection enhances the signal coming from the topmost layers with respect to the one coming from the bulk. The results are shown in Fig. 6, in which the ratios C_x /C_B, C_{O1}/C_B, C_{O2}/C_B of x-related and O-related contributions respect to the bulk contribution are displayed as a function of the emission angle (θ) with respect to the sample surface normal. Dotted lines are data fit functions of the form A/cos(θ) according to the Fadley's model, [64] where A is used as the fitting parameter for each component. It is evident how both the ratios of C_x component and the O-related components increase for grazing emission. These findings indicate that oxygen does not come from impurities inside the bulk diamond and that both the C_x and the O-related components are mostly distributed in the topmost surface layers.

We have estimated the x and O coverages by using the Fadley's model [64]: for x we have used C_x as the overlayer signal and C_B as the substrate signal; for O we have used the sum $C_{O1} + C_{O2}$ of the O-related components in the C1s spectra as the overlayer signal and the C_B component as the substrate signal. We have obtained an O coverage of (31 ± 3) % of the surface: the value is compatible with the fraction of diamond surface covered by O (33 ± 3) % estimated by comparing the O 1s and C 1s gross intensities (see discussion of Fig. 4), suggesting the reliability of the used approach. As far as the x coverage related to C_x intensity is concerned, it turns out to be (189 ± 19) %. This value should correspond to a thickness larger than a single layer. This result disagrees with Graupner's interpretation [67], where the thickness associated with the C_x component is at most one layer. Besides, Schenk identifies such a component with subsurface carbon not bound to hydrogen [68]. We propose instead that this component is ascribed to both surface and subsurface carbon atoms bound to hydrogen. In this scenario hydrogen atoms should be present also in the subsurface region. To put on a firm ground this hypothesis, we have performed Monte Carlo simulations of the hydrogenation plasma process. Results indicate a very weak dependence of the penetration depth of H particles on the impinging angle, between normal incidence and 45°. More relevant is the dependence on the equivalent potential difference. Simulations, performed from 100 V to 800 V (the maximum typical value in plasma reactor according to Moisan)[72], well represent the hydrogen plasma voltages used in this experiment, which are distributed up to 800 V. Results reported in Fig. 7 show a penetration depth distribution peaked at about 10 Å, 70 Å and 100 Å from the topmost layer for 100 V, 500 V and 800 V respectively. Thus, the hydrogenation process gives rise to C–H bond formation and/or to defects creation both in the diamond topmost [67] and underneath layers [26], whose presence is testified by the C_x component and due to the penetration of hydrogen ions into the solid during the plasma treatment. Lastly, the angle dependence of the XPS intensities of the C_x component means that the effects of hydrogen diffusion into the diamond lattice are limited to a few layers underneath the surface.

The fitting procedure applied to analyze C 1s line measured on the annealed surface has been also used in the case of the conductive surface, upon fixing the energy positions (apart from an overall rigid energy shift of 1.2 eV) of the different components. The best fit is displayed in Fig. 5b. In the comparative Table 1, the component absolute intensities show very small variations. More significantly, we can consider the

[1] Given our experimental resolution, we cannot be extremely precise on the position of the C_x component; anyway, if we use an energy shift of 0.36 eV,[66] analogue results have been obtained (see Supplementary material).

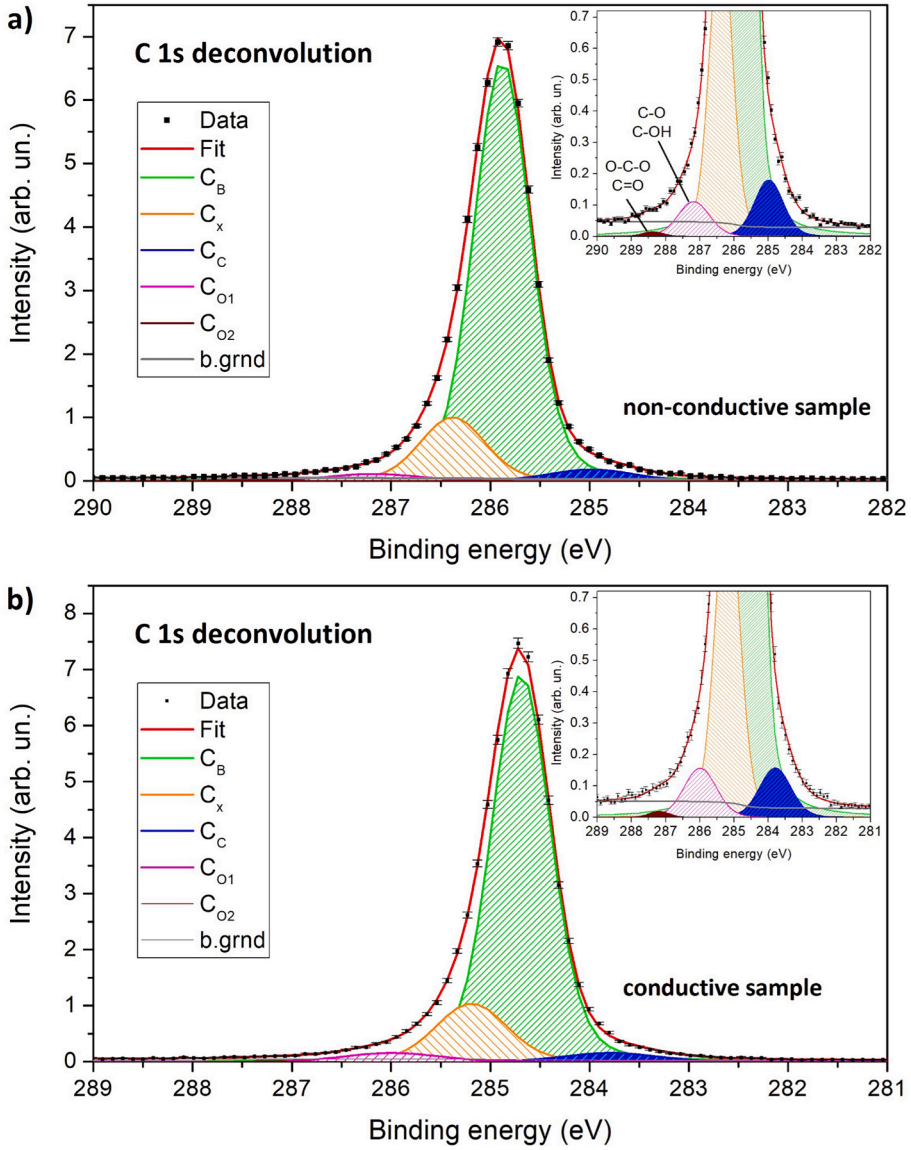

Fig. 5. Fits of the C 1s core level spectra measured on the HD surface: a) non-conductive sample, b) conductive sample. Peak assignments are the following: C_B is the bulk component, C_x is discussed in the text; C_C is due to surface carbon not bonded with hydrogen and to defects; C_{O1} and C_{O2} contributions (zoomed in the insets) are due to oxygen-bonded carbon (the respective bonds are also shown). Peak parameters are reported in Table 1.

variations of their ratios to the respective bulk component. In particular, the $I(C_x)/I(C_B)$ ratio is unchanged within 1 %, suggesting that the UHV annealing process to switch from conductive to non-conductive state produces no significant hydrogen loss, or atomic diffusion, as reasonably expected for the annealing temperature used (450 °C) [67]. In the conductive sample we have found that both the $I(C_{O1})/I(C_B)$ and the $I(C_{O2})/I(C_B)$ ratios are increased by about 30 % (see Table 1): being such components associated with oxygen-related sites, this finding agrees with the larger intensity of the O 1 s line discussed in Fig. 4, due to the presence of the "active" oxygen.

Given that "active" oxygen can contribute to the transfer-doping mechanism,[8,26,42,43] the next step in our investigation was then to individuate whether there is a preferential "active" oxygen bonding with carbon. To address this issue, we have investigated the evolution of the O-related site components distribution upon transition from non-conductive to conductive state by performing a deconvolution of the O 1s XPS line shape similarly to the C 1s core level analysis. By using results available in literature as a guide,[41,69] with reference to Fig. 8, where spectra measured on the non-conductive (panel a) and conductive (panel b) surfaces are displayed, four fit components have been used. In the non-conductive sample we have identified the following structures: O1 peak (at 533.7 eV binding energy) dominates the O 1s line and it is mainly due to O bonded in C-OH and CO configurations; O2 (at 535.0 eV) and O3 (at 532.4 eV) peaks are principally due to O bonded in long chains (such as OH-C=O or O-C=O) in which photo-emitted electrons come from single-bonded (O2) and double-bonded (O3) sites, respectively [41,69]. Upon transition from non-conductive to conductive state induced by air exposure, we observe a rigid energy shift of the components and an increase of the O1, O2 and O3 intensities components by about 30 %, accordingly with the discussion of Fig. 4. A further O component at 535.6 eV, labeled O4 peak, which is related to O in H_2O, though being a very minor contribution to oxygen overall intensity, becomes visible (notably, this component has an almost vanishing intensity in the non-conductive sample). Such evolution of the distribution of O-related site components would suggest that there is no preferred way for "active" O bonding with C.

To shed further light on the role of oxygen bond in the HD surface, we have exposed the annealed sample to oxygen in a controlled way (UHV conditions), both in molecular (O_2) and dissociated atomic form (O), by using the device described in the experimental section. The

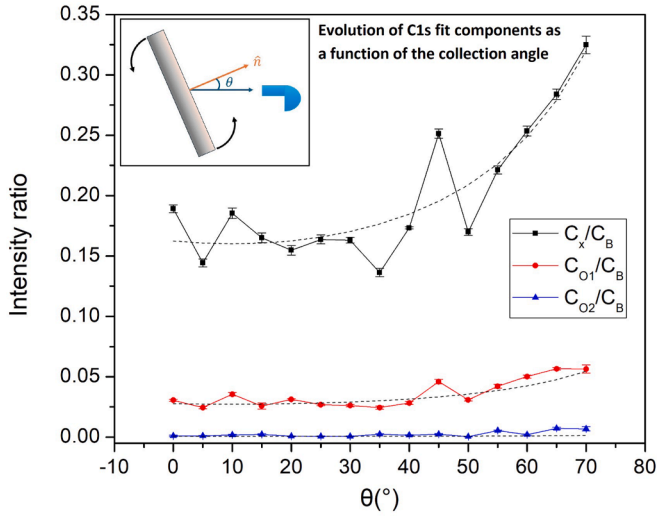

Fig. 6. Evolution of the ratios between the fit components and the bulk component of the C 1s in the non-conductive sample as a function of the collecting angle. Dotted lines represent the A/cos(θ) trend (θ being the emission angle with respect to the sample normal) according to the Fadley model [64].

exposure of the annealed surface to molecular oxygen up to of 10^4 L did not produce any change in the core level line shape. The results of surface exposure to atomic O, which are summarized in the spectra displayed in Fig. 9, are much different. The evolution of the O1s line is displayed as a function of the O exposure dose (Fig. 9 a), in which we can distinguish two effects. From the point of view of the energy position, a shift towards lower binding energies with respect to the non-conductive surface (annealed after air-exposure) is visible after the first exposure to 3000 L, with further slight variations after 6000 L and 9000 L exposures. At 9000 L the shift of the O1s core level saturates to a value of about 0.4 eV. The second aspect is the amount of oxygen monitored through the O1s peak intensity, which increased during the O-exposures, saturating again at 9000 L. According to these two findings, oxygen exposure does not replicate the air-exposure behavior, since peak energy and intensity are different from the ones of the air-exposed conductive sample.

We have also performed a thermal annealing on the O-exposed sample with the same parameters (temperature and pressure) used to anneal sample coming from air. Results are reported in Fig. 9b that shows a comparison of the O1s line for the O-exposed surface with the annealed-sample both after O-exposure and after air-exposure: while the energy positions of the annealed samples are similar, the annealed sample after O-exposure shows a higher intensity (about 50 %) than the annealed surface after air-exposure.

In order to explain this different behavior, we compare the evolution of the sum of the intensities of oxygen-related components in the C 1s core level ($C_{O1} + C_{O2}$), normalized to the C_B component area, with the overall intensity of the O 1s line (calculated by the O 1s area), for all the four cases studied (conductive sample from air, annealed after air-exposure, O-exposed, annealed after O-exposure). The result is displayed in Fig. 10, in which we have normalized both data sets to the value of sample annealed after air exposure, since, in principle, it represents the reference value due to the absence of physisorbed molecules on the surface. The evolution of the two sets is slightly different. Starting from the O 1s intensity, it can be noticed that the oxygen quantity significantly decreases from the conductive (air-exposed) to the non-conductive phase (annealed after air exposure); then the oxygen quantity is partially restored by O-exposure, and it does not change after re-annealing the sample. These findings are a different visualization of the results (relative to the intensity) reported in Fig. 9. However, the evolution of the O-related components in the C 1s line behaves differently: even if it shows a decrease of the oxygen quantity from conductive (air-exposure) to non-conductive (annealing) phase similarly to what happens to the O 1s total intensity. However, it does not show its partial restoration in the oxygen-exposed phase; the restoration, in fact, occurs only after the re-annealing treatment. We can interpret this particular

Table 1
Fit values of C 1s core level spectra of the non-conductive and conductive samples (fits are displayed in Fig. 5). For each component the binding energy (BE), the amplitude (I), the Gaussian widths (GW) and the Lorentzian (LW) widths are shown. Comparative intensities of the carbon-related components as relative ratios to C_B are reported in the last column.

Fit component	BE (eV)	I (arb. un.)	GW (eV)	LW (eV)	I/I(C_B)
Non-conductive sample					
C_B	285.9	5.18	0.59	0.15	1.000
C_x	286.4	0.89	0.69	0.15	0.172
C_C	285.0	0.20	0.92	0.15	0.038
C_{O1}	287.2	0.14	1.00	0.15	0.027
C_{O2}	288.4	0.01	0.66	0.15	0.002
Conductive sample					
C_B	284.7	5.65	0.62	0.15	1.000
C_x	285.2	1.00	0.76	0.15	0.177
C_C	283.8	0.19	1.01	0.15	0.034
C_{O1}	286.0	0.20	1.04	0.15	0.035
C_{O2}	287.2	0.02	0.66	0.15	0.004

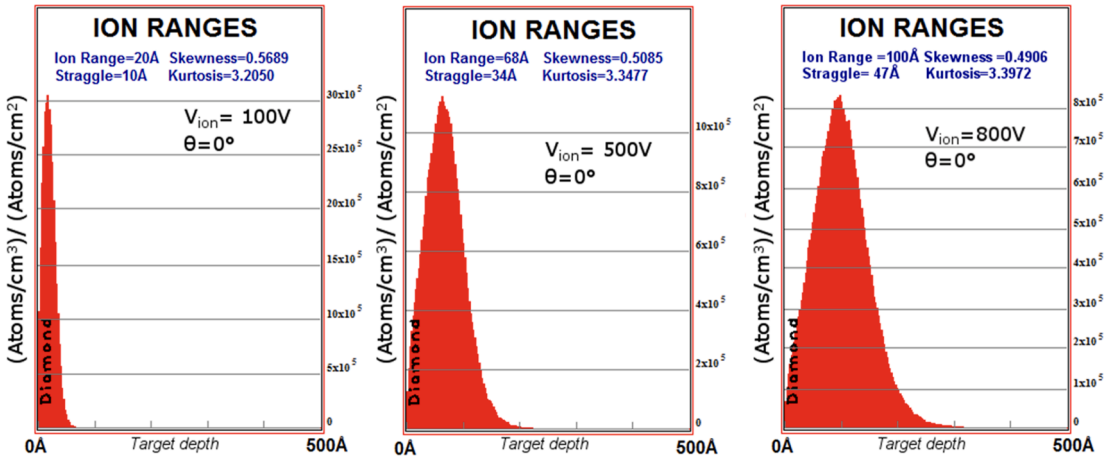

Fig. 7. Monte Carlo simulations of the penetration depth for hydrogen atoms into the diamond sample during plasma exposure: results are for normal impinging direction and relative to different reactor-sample potential differences.

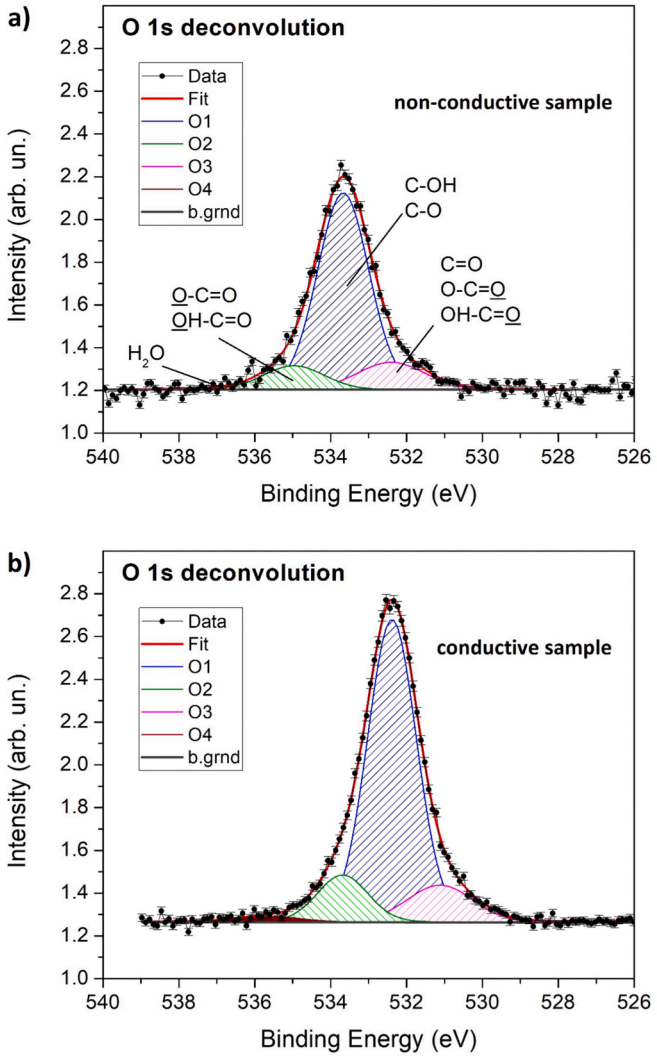

Fig. 8. Fit of the O 1s XPS line shape of the non-conductive (a) and conductive (b) states; details of the fit deconvolution can be found in the text; peak assignment has been done by using refs [41,69] as a guide.

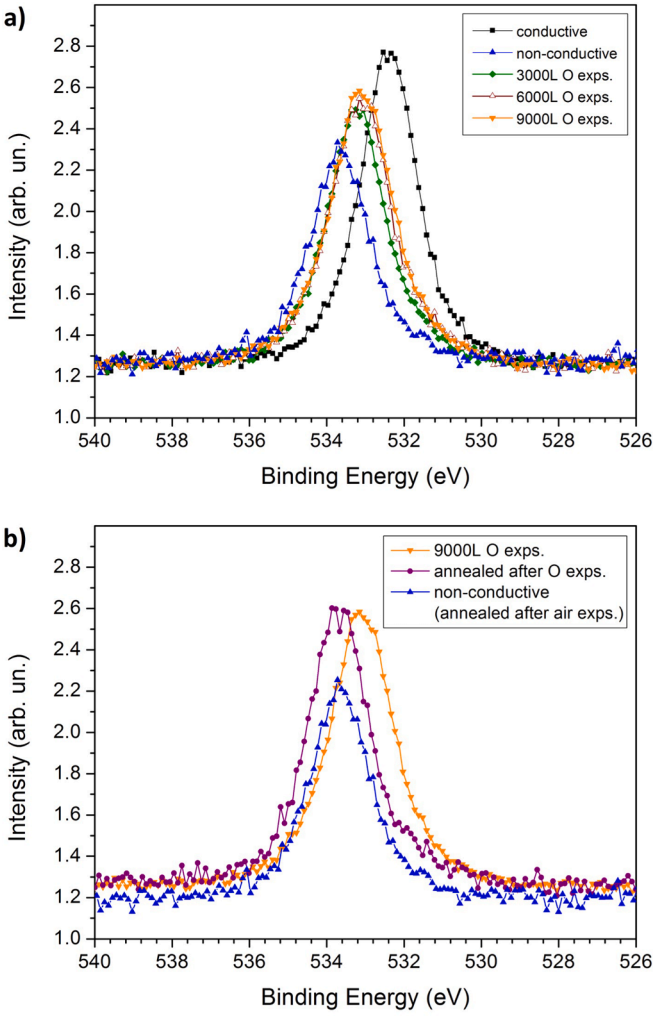

Fig. 9. (a) Evolution of the O 1s core level spectra measured on diamond non-conductive surface upon atomic O-exposure in steps of 3000 L (see text for details); the spectrum measured on the conductive (air-exposed) surface is also shown. (b) Comparison of spectra measured on the non-conductive (annealed after air exposure) surface, after 9000 L O-exposure and after re-annealing.

behavior in terms of different nature of the O-bonded species for the air-exposed and O-exposed cases: the curves, in fact, suggest the possibility that, while in the airborne species the oxygen atoms are principally bonded with carbon, this is no longer true for the oxygen cracked by filament, which binds with carbon on diamond surface only due to the thermal energy provided by re-annealing. This behavior raises the question of how oxygen atoms are bound with the HD surface in the case of oxygen exposure. A possible interpretation of our results can be found in literature by inferring the results of UV-oxidation of H-terminated nano-crystalline diamond films:[73,74] it has been shown that sample irradiation by UV source in pure O_2 atmosphere (similarly to filament cracking, UV radiation yields molecular dissociation) produces a high density of OH^- fragments which bond electrostatically with the CH terminations present at the surface. Hence it is not unreasonable that also in the case of filament cracking, several electrostatic $CH^+ \cdots OH^-$ bonds are formed (O atoms adsorb on the sample as a part of OH^- ions). Then the thermal activation produced by the annealing process could transform the bond between the OH^- ion and surface CH^+ termination into other bonds such as hydroxyl, carbonyl and ether-like bonds. Such a finding suggests that oxygen adsorption alone might not be responsible of inducing diamond SC. This may not appear as a surprise, since SC in hydrogen terminated diamond has also been observed with adsorbate layer not containing oxygen, such as fullerene and fluorinated fullerenes

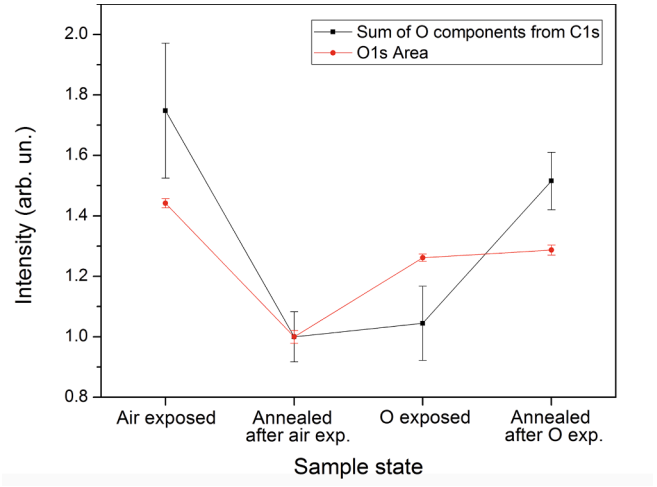

Fig. 10. Intensity comparison of O 1s core level and O-related components in C 1s core level for different sample treatments. On the ordinate axis the two sets are reported upon normalizing to one the value relative to the sample annealed after air exposure.

[75,76], polypyrrole [77], or more complicated architecture consisting of $C_{60}F_{48}$ and an intralayer of zinc-tetraphenylporphyrin [78]. The common picture that is generally put forward in order to explain the diamond SC, both in air-exposed and in these other types of adsorbates, is that the adsorbate layer behaves as strongly acceptor like. In this context our findings thus suggest that the presence of oxygen alone does not result in a molecular species with a sufficient acceptor behavior with respect to the hydrogen-terminated diamond surface. Only a more complicated molecular species, such as hydroxyl groups, and a surplus in energy supplied e.g. by the post-annealing process, give rise to an electronic configuration capable of inducing the appropriate behavior to obtain the expected two-dimensional conductivity.

4. Conclusions

An accurate investigation of the morphology and electronic structure of plasma-hydrogenated diamond (100) surface correlated to its conductivity state has been performed by using electron diffraction and spectroscopies. Such techniques have allowed us to provide a deeper understanding of the role of adsorbates in altering the morphological and electronic properties of the surface and at the same time to accurately quantify the presence of chemical species, such as the presence of spurious oxygen due to the sample preparation and not completely removed during the hydrogenation treatment.

On the non-conductive (annealed) surface, SA-LEED analysis [52,53] has estimated the diameter of hydrogenated diamond coherently scattering domains to be of the order of tens of Angstroms. A refined XPS analysis supported by Monte Carlo simulations has suggested the presence of hydrogen bonded to carbon also in the subsurface region.

On the conductive surface (air-exposed sample), the 1.5 eV shift of the surface plasmon, measured by EELS, has been attributed to the presence of adsorbates. These adsorbates are randomly arranged on the sample surface, as can be evinced by SA-LEED, and, according to XPS results, cover about 23 % of the surface. This coverage is responsible for the surface conductivity.

The analysis of the O 1s line shape suggests no preferential O-bonding for the adsorbates; however, the C 1s analysis reveals that at least a fraction of these adsorbates bond with C via an O atom.

Finally, the controlled oxygen exposure of the HD surface, both in molecular (O_2), and dissociated atomic form (O), has shown that O_2 does not react and O adsorbs on the surface without bonding to C at RT, differently from the airborne adsorbates that are responsible for surface conductivity.

Declaration of Generative AI and AI-assisted technologies in the writing process

During the preparation of this work D.P. used openAI/chatGPT in order to improve readability and language. After using this tool, the author reviewed and edited the content as needed and takes full responsibility for the content of the publication.

CRediT authorship contribution statement

Stefano Iacobucci: Writing – review & editing, Writing – original draft, Visualization, Supervision, Project administration, Methodology, Investigation, Conceptualization. **Valerio Serpente:** Writing – review & editing, Writing – original draft, Visualization, Validation, Software, Methodology, Investigation, Formal analysis, Data curation, Conceptualization. **Daniele Paoloni:** Writing – review & editing, Writing – original draft, Visualization, Software, Formal analysis, Data curation, Conceptualization. **Daniele M. Trucchi:** Writing – review & editing, Supervision, Resources, Project administration, Methodology, Conceptualization. **Francesco Offi:** Writing – review & editing, Conceptualization. **Alessandro Ruocco:** Writing – review & editing, Supervision, Resources, Project administration, Methodology, Investigation, Conceptualization.

Declaration of competing interest

The authors declare that they have no known competing financial interests or personal relationships that could have appeared to influence the work reported in this paper.

Acknowledgments

The Convenzione Operativa “Tecnologie quantistiche per lo studio di sistemi alla nanoscala rilevanti alla realizzazione di applicazioni sensoristiche biomedicali, magnetiche ed elettroniche” between CNR-ISM and Dipartimento di Scienze of Università Roma Tre is acknowledged.

Appendix A. Supplementary data

Supplementary data to this article can be found online at https://doi.org/10.1016/j.apsusc.2025.162688.

Data availability

Data will be made available on request.

References

[1] C. Wort, R. Balmer, Diamond as an electronic material, Mater. Today 11 (1–2) (2008) 22–28, https://doi.org/10.1016/S1369-7021(07)70349-8.
[2] C. Nebel, J. Ristein, Thin-Film Diamond I:(part of the Semiconductors and Semimetals Series), Academic Press, 2003.
[3] C. Nebel, B. Rezek, D. Shin, H. Uetsuka, N. Yang, Diamond for bio-sensor applications, J. Phys. D Appl. Phys. 40 (20) (2007) 6443, https://doi.org/10.1088/0022-3727/40/20/S21.
[4] T. Sun, F. Koeck, C. Zhu, R. Nemanich, Combined visible light photo-emission and low temperature thermionic emission from nitrogen doped diamond films, Appl. Phys. Lett. 99 (20) (2011), https://doi.org/10.1063/1.3658638.
[5] D. Trucchi, A. Bellucci, M. Girolami, P. Calvani, E. Cappelli, S. Orlando, R. Polini, L. Silvestroni, D. Sciti, A. Kribus, Solar thermionic-thermoelectric generator (ST2G): concept, materials engineering, and prototype demonstration, Adv. Energy Mater. 8 (32) (2018) 1802310, https://doi.org/10.1002/aenm.201802310.
[6] P. Calvani, A. Bellucci, M. Girolami, S. Orlando, V. Valentini, R. Polini, D. Trucchi, Black diamond for solar energy conversion, Carbon 105 (2016) 401–407, https://doi.org/10.1016/j.carbon.2016.04.017.
[7] M. Girolami, A. Bellucci, M. Mastellone, S. Orlando, V. Valentini, R. Montereali, M. Vincenti, R. Polini, D. Trucchi, Optical characterization of double-nanotextured black diamond films, Carbon 138 (2018) 384–389, https://doi.org/10.1016/j.carbon.2018.07.055.
[8] F. Maier, M. Riedel, B. Mantel, J. Ristein, L. Ley, Origin of surface conductivity in diamond, Phys. Rev. Lett. 85 (16) (2000) 3472, https://doi.org/10.1103/PhysRevLett.85.3472.
[9] M. Landstrass, K. Ravi, Resistivity of chemical vapor deposited diamond films, Appl. Phys. Lett. 55 (10) (1989) 975–977, https://doi.org/10.1063/1.101694.
[10] M. Hauf, P. Simon, M. Seifert, A. Holleitner, M. Stutzmann, J. Garrido, Low dimensionality of the surface conductivity of diamond, Phys. Rev. B 89 (11) (2014) 115426, https://doi.org/10.1103/PhysRevB.89.115426.
[11] G. Conte, E. Giovine, A. Bolshakov, V. Ralchenko, V. Konov, Surface channel MESFETs on hydrogenated diamond, Nanotechnology 23 (2) (2011) 025201, https://doi.org/10.1088/0957-4484/23/2/025201.
[12] Z. Ren, D. Lv, J. Xu, J. Zhang, J. Zhang, K. Su, C. Zhang, Y. Hao, High temperature (300 C) ALD grown Al2O3 on hydrogen terminated diamond: Band offset and electrical properties of the MOSFETs, Appl. Phys. Lett. 116 (1) (2020), https://doi.org/10.1063/1.5126359.
[13] G. Akhgar, O. Klochan, L. Beveren, M. Edmonds, F. Maier, B. Spencer, J. McCallum, L. Ley, A. Hamilton, C. Pakes, Strong and tunable spin–orbit coupling in a two-dimensional hole gas in ionic-liquid gated diamond devices, Nano Lett 16 (6) (2016) 3768–3773, https://doi.org/10.1021/acs.nanolett.6b01155.
[14] K. Crawford, L. Cao, D. Qi, A. Tallaire, E. Limiti, C. Verona, A. Wee, D. Moran, Enhanced surface transfer doping of diamond by V2O5 with improved thermal stability, Appl. Phys. Lett. 108 (4) (2016), https://doi.org/10.1063/1.4940749.
[15] B. Koslowski, S. Strobel, P. Ziemann, Comment on “Origin of Surface Conductivity in Diamond”, Phys. Rev. Lett. 87 (20) (2001) 209705 https://doi.org/10.1103/PhysRevLett.87.209705.
[16] C. Nebel, Surface-conducting diamond, Science 318 (5855) (2007) 1391–1392, https://doi.org/10.1126/science.1151314.
[17] Y. Takagi, K. Shiraishi, M. Kasu, H. Sato, Mechanism of hole doping into hydrogen terminated diamond by the adsorption of inorganic molecule, Surf. Sci. 609 (2013) 203–206, https://doi.org/10.1016/j.susc.2012.12.015.

[18] T. Wade, M. Geis, T. Fedynyshyn, S. Vitale, J. Varghese, D. Lennon, T. Grotjohn, R. Nemanich, M. Hollis, Effect of surface roughness and H–termination chemistry on diamond's semiconducting surface conductance, Diam. Relat. Mater. 76 (2017) 79–85, https://doi.org/10.1016/j.diamond.2017.04.012.

[19] V. Chakrapani, J. Angus, A. Anderson, S. Wolter, B. Stoner, G. Sumanasekera, Charge transfer equilibria between diamond and an aqueous oxygen electrochemical redox couple, Science 318 (5855) (2007) 1424–1430, https://doi.org/10.1126/science.1148841.

[20] L. Ley, J. Ristein, F. Meier, M. Riedel, P. Strobel, Surface conductivity of the diamond: a novel transfer doping mechanism, Phys. B Condens. Matter 376 (2006) 262–267, https://doi.org/10.1016/j.physb.2005.12.068.

[21] S. Iacobucci, P. Alippi, P. Calvani, M. Girolami, F. Offi, L. Petaccia, D. Trucchi, Electronic structure of hydrogenated diamond: Microscopical insight into surface conductivity, Phys. Rev. B 94 (4) (2016) 045307, https://doi.org/10.1103/PhysRevB.94.045307.

[22] A. Hoffman, J. Foord, Hydrogen interactions with diamond. Physical Chemistry Chemical Physics, 13(24), p.11469–11470. and ref's therein, 2011, doi: 10.1039/C1CP90071D.

[23] F. Maier, J. Ristein, L. Ley, Electron affinity of plasma-hydrogenated and chemically oxidized diamond (100) surfaces, Phys. Rev. B 64 (16) (2001) 165411, https://doi.org/10.1103/PhysRevB.64.165411.

[24] J. Robertson, M. Rutter, Band diagram of diamond and diamond-like carbon surfaces, Diam. Relat. Mater. 7 (2–5) (1998) 620–625, https://doi.org/10.1016/S0925-9635(97)00257-4.

[25] J. Ristein, Surface science of diamond: Familiar and amazing, Surf. Sci. 600 (18) (2006) 3677–3689, https://doi.org/10.1016/j.susc.2006.01.087.

[26] K. Bobrov, A. Mayne, G. Comtet, G. Dujardin, L. Hellner, A. Hoffman, Atomic-scale visualization and surface electronic structure of the hydrogenated diamond C (100)-(2x1): H surface, Phys. Rev. B 68 (19) (2003) 195416, https://doi.org/10.1103/PhysRevB.68.195416.

[27] F. Liu, Y. Cui, M. Qu, J. Di, Effects of hydrogen atoms on surface conductivity of diamond film, AIP Adv. 5 (4) (2015), https://doi.org/10.1063/1.4904057.

[28] J. Goss, R. Jones, M. Heggie, C. Ewels, P. Briddon, S. Oberg, Theory of hydrogen in diamond, Phys. Rev. B 65 (11) (2002) 115207, https://doi.org/10.1103/PhysRevB.65.115207.

[29] C. Sauerer, F. Ertl, C. Nebel, M. Stutzmann, P. Bergonzo, O. Williams, R. Jackman, Low temperature surface conductivity of hydrogenated diamond, Physica Status Solidi (a) 186 (2) (2001) 241–247, https://doi.org/10.1002/1521-396X(200108)186:2<241::AID-PSSA241>3.0.CO;2-1.

[30] M. Kubovic, M. Kasu, Enhancement and stabilization of hole concentration of hydrogen-terminated diamond surface using ozone adsorbates, Jpn. J. Appl. Phys. 49 (11R) (2010), https://doi.org/10.1143/JJAP.49.110208.

[31] M. Geis, T. Fedynyshyn, M. Plaut, T. Wade, C. Wuorio, S. Vitale, J. Varghese, T. Grotjohn, R. Nemanich, M. Hollis, Chemical and semiconducting properties of NO2-activated H-terminated diamond, Diam. Relat. Mater. 84 (2018) 86–94, https://doi.org/10.1016/j.diamond.2018.03.002.

[32] H. Sato, M. Kasu, Electronic properties of H-terminated diamond during NO2 and O3 adsorption and desorption, Diam. Relat. Mater. 24 (2012) 99–103, https://doi.org/10.1016/j.diamond.2011.12.004.

[33] R. Flammini, M. Satta, A. Bellucci, M. Girolami, F. Wiame, D. Trucchi, Water desorption effects on the surface electrical resistance of air-exposed hydrogenated diamond, Applied Surface Science 512 (2020) 145491, https://doi.org/10.1016/j.apsusc.2020.145491.

[34] M. Kalutara Koralalage, R. Parish, A. Bates, S. McNamara, W. Paxton, G. Sumanasekera, The Influence of Absorbate Desorption and Kinetic Isotope Effects on the Surface Conductivity of Diamond, Journal of Electronic Materials 51 (6) (2022) 3336–3341, https://doi.org/10.1007/s11664-022-09594-8.

[35] M. Tordjman, C. Saguy, A. Bolker, R. Kalish, Superior surface transfer doping of diamond with MoO3, Adv. Mater. Interfaces 1 (3) (2014) 1300155, https://doi.org/10.1002/admi.201300155.

[36] M. Tordjman, K. Weinfeld, R. Kalish, Boosting surface charge-transfer doping efficiency and robustness of diamond with WO3 and ReO3, Appl. Phys. Lett. 111 (11) (2017), https://doi.org/10.1063/1.4986339.

[37] K. Xing, Y. Xiang, M. Jiang, D. Creedon, G. Akhgar, S. Yianni, H. Xiao, L. Ley, A. Stacey, J. McCallum, et al., MoO3 induces p-type surface conductivity by surface transfer doping in diamond, Appl. Surf. Sci. 509 (2020) 144890, https://doi.org/10.1016/j.apsusc.2019.144890.

[38] J. McGhee, V. Georgiev, Simulation study of surface transfer doping of hydrogenated diamond by MoO3 and V2O5 metal oxides, Micromachines 11 (4) (2020) 433, https://doi.org/10.3390/mi11040433.

[39] P. Strobel, M. Riedel, J. Ristein, L. Ley, Surface transfer doping of diamond, Nature 430 (6998) (2004) 439–441, https://doi.org/10.1038/nature02751.

[40] K. Xing, W. Li, E. Della Gaspera, J. Embden, L. Zhang, S. Yianni, D. Creedon, T. Wang, J. McCallum, L. Wang, et al., Surface transfer doping of diamond using solution-processed molybdenum trioxide, Carbon 175 (2021) 20–26, https://doi.org/10.1016/j.apsusc.2019.144890.

[41] N. Makau, T. Derry, Study of oxygen on the three low index diamond surfaces by XPS, Surf. Rev. Lett. 10 (02n03) (2003) 295–301, https://doi.org/10.1142/S0218625X03005189.

[42] S. Sque, R. Jones, P. Briddon, Structure, electronics, and interaction of hydrogen and oxygen on diamond surfaces, Phys. Rev. B—Condens. Matter Mater. Phys. 73 (8) (2006) 085313, https://doi.org/10.1103/PhysRevB.73.085313.

[43] M. Riedel, J. Ristein, L. Ley, Recovery of surface conductivity of H-terminated diamond after thermal annealing in vacuum, Phys. Rev. B 69 (12) (2004) 125338, https://doi.org/10.1103/PhysRevB.69.125338.

[44] K. Crawford, I. Maini, D. Macdonald, D. Moran, Surface transfer doping of diamond: a review, Prog. Surf. Sci. 96 (1) (2021) 100613, https://doi.org/10.1103/PhysRevB.69.125338.

[45] M. Edmonds, L. Beveren, O. Klochan, J. Cervenka, K. Ganesan, S. Prawer, L. Ley, A. Hamilton, C. Pakes, Spin–orbit interaction in a two-dimensional hole gas at the surface of hydrogenated diamond, Nano Lett 15 (1) (2015) 16–20, https://doi.org/10.1021/nl502081y.

[46] S. Kaciulis, A. Mezzi, P. Calvani, D. Trucchi, Electron spectroscopy of the main allotropes of carbon, Surf. Interface Anal. 46 (10–11) (2014) 966–969, https://doi.org/10.1002/sia.5382.

[47] J.F Ziegler, SRIM—The Stopping and Range of Ions in Matter., 2013, http://www.srim.org/.

[48] V. Serpente, Role of the Atmospheric Adsorbates in the Surface Conductivity of Hydrogen-Terminated Diamond, Università degli Studi Roma Tre, 2018. Doctoral dissertation.

[49] V. Serpente, A. Bellucci, M. Girolami, M. Mastellone, S. Iacobucci, A. Ruocco, D. Trucchi, Combined electrical resistivity-electron reflectivity measurements for evaluating the homogeneity of hydrogen-terminated diamond surfaces, Diam. Relat. Mater. 114 (2021) 108290, https://doi.org/10.1016/j.diamond.2021.108290.

[50] G. Pierantozzi, M. Sbroscia, A. Ruocco, Templating effect of the substrate on the structure of Cu-phthalocyanine thin film, Surf. Sci. 669 (2018) 176–182, https://doi.org/10.1016/j.susc.2017.12.003.

[51] E. Maydell, E. Dunlop, D. Fabian, J. Haupt, W. Gissler, Electron energy loss study of diamond-like and amorphous carbon films, Diam. Relat. Mater. 2 (5–7) (1993) 873–878, https://doi.org/10.1016/0925-9635(93)90242-T.

[52] D. Paoloni, A. Ruocco, Cu-phthalocyanine long-range ordered bulk growth due to the weak interaction with highly oriented pyrolytic graphite substrate, Surf. Sci. 735 (2023) 122322, https://doi.org/10.1016/j.susc.2023.122322.

[53] L. Persichetti, D. Paoloni, A. Apponi, L. Camilli, A. Caporale, V. Babenko, S. Hofmann, M. Angelucci, R. Cimino, M. De Seta, et al., Probing post-growth hydrogen intercalation and H2 nanobubbles formation in graphene on Ge (110), Mater. Sci. Semicond. Process. 173 (2024) 108111, https://doi.org/10.1016/j.mssp.2024.108111.

[54] V. Smentkowski, J. Yates Jr, Purity of atomic oxygen production from heated iridium surfaces, J. Vac. Sci. Technol. A 12 (1) (1994) 219–223, https://doi.org/10.1116/1.578886.

[55] X. Liu, L. Yang, Z. Hou, B. Da, K. Nagata, H. Yoshikawa, S. Tanuma, Y. Sun, Z. Ding, Machine learning approach for the prediction of electron inelastic mean free paths, Phys. Rev. Mater. 5 (3) (2021) 033802, https://doi.org/10.1103/PhysRevMaterials.5.033802.

[56] Y. Wang, K. Wong, S. Lee, M. Nishitani-Gamo, I. Sakaguchi, K. Loh, T. Ando, Surface structure of C (100)-(2x1)- H studied by a quantitative LEED analysis, Phys. Rev. B 59 (15) (1999) 10347, https://doi.org/10.1103/PhysRevB.59.10347.

[57] M. Henzler, LEED studies of surface imperfections, Appl. Surf. Sci. 11 (1982) 450–469, https://doi.org/10.1016/0378-5963(82)90092-7.

[58] T. Mercer, P. Pehrsson, Surface state transitions on the reconstructed diamond C (100) surface, Surf. Sci. 399 (1) (1998) L327–L331.

[59] P. Pehrsson, T. Mercer, Oxidation of heated diamond C (100): H surfaces, Surf. Sci. 460 (1–3) (2000) 74–90, https://doi.org/10.1016/S0039-6028(00)00495-7.

[60] Y. Wang, H. Chen, R. Hoffman, J. Angus, Structural analysis of hydrogenated diamond-like carbon films from electron energy loss spectroscopy, J. Mater. Res. 5 (11) (1990) 2378–2386, https://doi.org/10.1557/JMR.1990.2378.

[61] Y. Fan, A. Fitzgerald, P. John, C. Troupe, J. Wilson, X-ray photoelectron spectroscopy studies of CVD diamond films, Surf. Interface Anal.: Int. J. Devoted to the Development and Application of Techniques for the Analysis of Surfaces, Interfaces and Thin Films 34 (1) (2002) 703–707, https://doi.org/10.1002/sia.1392.

[62] A. Ruocco, M. Donzello, F. Evangelista, G. Stefani, Relevance of the electron energy-loss spectroscopy for in situ studies of the growth mechanism of copper phthalocyanine molecules on metal surfaces: Al (100), Phys. Rev. B 67 (15) (2003) 155408, https://doi.org/10.1103/PhysRevB.67.155408.

[63] H. Raether, Excitation of Plasmons and Interband Transitions by Electrons, vol. 88, Springer, 2006.

[64] C. Fadley, electron spectroscopy theory techniques and applications, Academic Press, 1978.

[65] S. Tanuma, C. Powell, D. Penn, Calculations of electron inelastic mean free paths. IX. Data for 41 elemental solids over the 50 eV to 30 keV range, Surf. Interface Anal. 43 (3) (2011) 689–713, https://doi.org/10.1002/sia.3522.

[66] C. Verona, W. Ciccognani, S. Colangeli, E. Limiti, M. Marinelli, G. Verona-Rinati, Comparative investigation of surface transfer doping of hydrogen terminated diamond by high electron affinity insulators, J. Appl. Phys. 120 (2016) 025104, https://doi.org/10.1063/1.4955469.

[67] R. Graupner, F. Maier, J. Ristein, L. Ley, C. Jung, High-resolution surface-sensitive C 1 s core-level spectra of clean and hydrogen-terminated diamond (100) and (111) surfaces, Phys. Rev. B 57 (19) (1998) 12397, https://doi.org/10.1103/PhysRevB.57.12397.

[68] A. Schenk, K. Rietwyk, A. Tadich, A. Stacey, L. Ley, C. Pakes, High resolution core level spectroscopy of hydrogen-terminated (1 0 0) diamond, J. Phys. Condens. Matter 28 (30) (2016) 305001, https://doi.org/10.1088/0953-8984/28/30/305001.

[69] S. Petrick, C. Benndorf, Potassium adsorption on hydrogen-and oxygen-terminated diamond (100) surfaces, Diam. Relat. Mater. 10 (3–7) (2001) 519–525, https://doi.org/10.1016/S0925-9635(00)00440-4.

[70] F. Klauser, S. Ghodbane, R. Boukherroub, S. Szunerits, D. Steinmuller-Nethl, E. Bertel, N. Memmel, Comparison of different oxidation techniques on single-

crystal and nanocrystalline diamond surfaces, Diam. Relat. Mater. 19 (5–6) (2010) 474–478, https://doi.org/10.1016/j.diamond.2009.11.013.
[71] P. John, M. Stoikou, Hydrogen plasma interaction with (100) diamond surfaces, PCCP 13 (24) (2011) 11503–11510, https://doi.org/10.1039/C1CP20099B.
[72] M. Moisan, M. Wertheimer, Comparison of microwave and rf plasmas: fundamentals and applications, Surf. Coat. Technol. 59 (1–3) (1993) 1–13, https://doi.org/10.1016/0257-8972(93)90047-R.
[73] G. Speranza, S. Torrengo, A. Miotello, L. Minati, I. Bernagozzi, M. Ferrari, M. Dipalo, E. Kohn, XPS and UPS in situ study of oxygen thermal desorption from nanocrystalline diamond surface oxidized by different process, Diam. Relat. Mater. 20 (4) (2011) 560–563, https://doi.org/10.1016/j.diamond.2011.03.001.
[74] S. Torrengo, R. Canteri, R. Dell'Anna, L. Minati, A. Pasquarelli, G. Speranza, XPS and ToF-SIMS investigation of nanocrystalline diamond oxidized surfaces, Appl. Surf. Sci. 276 (2013) 101–111, https://doi.org/10.1016/j.apsusc.2013.03.041.
[75] P. Strobel, M. Riedel, J. Ristein, L. Ley, Surface transfer doping of diamond, Nature 430 (2004) 439–441, https://doi.org/10.1038/nature02751.
[76] M.T. Edmonds, M. Wanke, A. Tadich, H.M. Vulling, K.J. Rietwyk, P.L. Sharp, C. B. Stark, Y. Smets, A. Schenk, Q.-H. Wu, L. Ley, C.I. Pakes, Surface transfer doping of hydrogen-terminated diamond by C60F48: Energy level scheme and doping efficiency, J. Chem. Phys. 136 (12) (2012), https://doi.org/10.1063/1.3695643.
[77] E. Ukraintsev, A. Kromka, W. Janssen, K. Haenen, D. Takeuchi, P. Bábor, B. Rezek, Electron emission from H-terminated diamond enhanced by polypyrrole grafting, Carbon 176 (2021) 642–649, https://doi.org/10.1016/j.carbon.2020.12.043.
[78] D.P. Langley, Y. Smets, C.B. Stark, M.T. Edmonds, A. Tadich, K.J. Rietwyk, A. Schenk, M. Wanke, Q.-H. Wu, P. Barnard, L. Ley, C.I. Pakes, Surface transfer doping of diamond with a molecular heterojunction, Appl. Phys. Lett. 100 (2012) (2012), https://doi.org/10.1063/1.3676445.